

 Open access • Journal Article • DOI:10.1038/NMAT4802

Buckled two-dimensional Xene sheets — [Source link](#)

[Alessandro Molle](#), [Joshua E. Goldberger](#), [Michel Houssa](#), [Yong Xu](#) ...+2 more authors





Institutions: [Olivetti](#), [Ohio State University](#), [Katholieke Universiteit Leuven](#), [Tsinghua University](#) ...+2 more institutions

Published on: 01 Feb 2017 - [Nature Materials](#) (Nature Publishing Group)

Topics: [Germanene](#), [Stanene](#), [Silicene](#), [Topological insulator](#) and [Electronic structure](#)

Related papers:

- [Electric Field Effect in Atomically Thin Carbon Films](#)
- [Generalized Gradient Approximation Made Simple](#)
- [Epitaxial growth of two-dimensional stanene](#)
- [Silicene: Compelling Experimental Evidence for Graphenelike Two-Dimensional Silicon](#)
- [Efficient iterative schemes for ab initio total-energy calculations using a plane-wave basis set.](#)

Share this paper:    

View more about this paper here: <https://typeset.io/papers/buckled-two-dimensional-xene-sheets-4d6zr0j0d4>

Buckled Two-Dimensional Xene Sheets

Alessandro Molle¹, Joshua Goldberger², Michel Houssa³, Yong Xu^{4,5,6}, Shou-Cheng Zhang^{7,8,9}, and Deji Akinwande¹⁰

¹ Laboratorio MDM, IMM-CNR, via C. Olivetti 2, Agrate Brianza, I-20864, Italy

² Department of Chemistry and Biochemistry, The Ohio State University, Columbus, OH 43210, USA

³ Department of Physics and Astronomy, University of Leuven, B-3001 Leuven, Belgium

⁴ State Key Laboratory of Low Dimensional Quantum Physics, Department of Physics, Tsinghua University, Beijing 100084, People's Republic of China

⁵ Collaborative Innovation Center of Quantum Matter, Beijing 100084, People's Republic of China

⁶ RIKEN Center for Emergent Matter Science (CEMS), Wako, Saitama 351-0198, Japan

⁷ Department of Physics, McCullough Building, Stanford University, Stanford, California 94305-4045, USA

⁸ Stanford Institute for Materials and Energy Sciences, SLAC National Accelerator Laboratory, Menlo Park, California 94025, USA

⁹ Institute for Advanced Study, Tsinghua University, Beijing 100084, People's Republic of China

¹⁰ Microelectronics Research Center, The University of Texas at Austin, Texas 78758, USA

33

34

Abstract

35 Silicene, germanene, and stanene, are part of a monoelemental class of two-dimensional
36 (2D) crystals termed 2D-Xenes ($X=Si, Ge, Sn$) which, together with their ligand-
37 functionalized derivatives referred to as Xanes, are comprised of group IVA atoms
38 arranged in a honeycomb lattice – similar to graphene but with varying degrees of
39 buckling. Their electronic structure range from trivial insulators, to semiconductors with
40 tunable gaps, to semimetallic, depending on the substrate, chemical functionalization, and
41 strain. More than a dozen different topological insulator states are predicted to emerge,
42 including the quantum spin Hall state at room temperature, which, if realized, would
43 enable new classes of nanoelectronic and spintronic devices, such as the topological field
44 effect transistor. The electronic structure can be tuned, for example, by changing the
45 group IVA element, the degree of spin-orbit coupling, the functionalization chemistry, or
46 the substrate, making the 2D-Xene systems promising multifunctional 2D materials for
47 nanotechnology. This Perspective Article highlights the current state-of-the art and future
48 opportunities in the manipulation and stability of these materials, their functions and
49 applications, and novel device concepts.

50

51

52

53

54

55 The rise of graphene has inspired the flourish of a so-called “flatland” of two-
56 dimensional (2D) materials with complementary properties and functionalities enabling
57 rapid advances in science and engineering, and an accelerated global development in
58 nanotechnology applications that can address societal challenges in energy, electronics,
59 sensors and health.^{1,2,3} One closely related class of 2D crystals are the single-element
60 “2D-Xenes”, which take their etymology from the sp^2 -hybridized alkene bond and are
61 generally comprised of a single-layer of atoms organized into a honeycomb-like lattice.
62 In particular, 2D-Xenes made of group-IVA elements, referred to as “silicene”,
63 “germanene”, and “stanene” when X=Si, Ge, and Sn respectively, are isoelectronic to
64 graphene,⁴ however their larger interatomic distances result in up and down atomic
65 buckling about a honeycomb lattice⁵, and also afford new routes towards covalent
66 functionalization. The buckled structure and the strong spin-orbit coupling (SOC)
67 concurrently paves a pathway for accessing the new quantum state of matter known as a
68 2D topological insulator (TI), a solid-state material that has both an insulating electronic
69 structure in the bulk and dissipation-less conducting channels along the edges that are
70 protected against back-scattering by time reversal symmetry. The potential technological
71 value of such an effect is that it enables the creation of a material that exhibits ideal
72 conduction along the edges that is immune from scattering from a variety of defects and
73 disorder. Overall, intriguing questions have come to the forefront such as: What are the
74 benefits and challenges that arise owing to the intrinsic buckling and surface sensitivity in
75 2D-Xenes? And can 2D-Xenes ultimately establish topology as a paradigm shift for
76 nanoscale opto-electronics? These questions are discussed here with highlights on the
77 opportunities and perspectives on the technical challenges.

78 **A pseudo planar flatland**

79

80 While the planar flatland has been considered the norm for the past ten years as is the
81 case for graphene and h-BN, *anisotropy* in honeycomb lattices stemming from the
82 extended vertical distortions (for example bond buckling in 2D-Xenes or puckering in
83 phosphorene) is now the *new normal*.^{4,5,6} The native buckling can have dramatic
84 implications in the overall physics and chemistry of the 2D-Xenes. For instance, the
85 degree of buckling can dictate the electronic character or influence the chemical
86 reactivity. This highlights the concept of a pseudo-planar flatland where buckling can
87 foster a number of potential functionalities that can be readily engineered.

88 **An in-depth view on buckling.** In their most stable form, 2D-Xenes based on Si, Ge
89 or Sn atoms adopt a buckled hexagonal honeycomb structure^{6,7}, unlike graphene, which is
90 ideally flat. For example, the larger bond length in silicene (~ 2.28 Å) compared to
91 graphene (~ 1.42 Å), prevents the Si atoms from forming strong π -bonds, thus leading to
92 deviations away from a sp^2 hybridization.^{4,8} The buckling of the Si atoms brings them
93 closer together to enable a stronger overlap of their π -bonding p_z orbitals, resulting in a
94 mixed sp^2 - sp^3 hybridization, which stabilizes their hexagonal arrangement. The vertical
95 buckling distance δ between the top and bottom atoms of the 2D-Xene crystal structure
96 (**Figure 1a**) is correlated to the bond angle between the framework atoms and the
97 hybridization of the atomic orbitals: δ increases from 0 Å in graphene to 0.85 Å in free-
98 standing (FS) stanene, with an associated decrease of the bond angle, from 120° (pure sp^2
99 hybridization of C atoms) to 110° (almost pure sp^3 hybridization of Sn atoms).

100 2D-Xenes can be described by a four-band second-nearest neighbor tight binding
 101 Hamiltonian⁹ near the K and K' points, involving a SOC term (λ_{SO}) and a staggered
 102 external electric field term (E_z),

$$103 \quad H = \hbar v_F (\eta k_x \tau_x + k_y \tau_y) + \eta \tau_z \sigma_z \lambda_{SO} - \frac{\delta}{2} E_z \tau_z + \frac{\lambda_{R1} (\eta \tau_x \sigma_y - \tau_y \sigma_x)}{2} + \eta \tau_z a \lambda_{R2} (k_y \sigma_x -$$

$$104 \quad k_x \sigma_y), \quad (1)$$

105 where v_F is the Fermi velocity, $\eta=1$ for K and $\eta=-1$ for K' point, $\tau_{x,y,z}$ is the Pauli matrix
 106 for the sublattice pseudospin, σ is the Pauli matrix for the electron spin, and λ_{R1} and λ_{R2}
 107 are the first and second Rashba coupling constants, related to the nearest and second
 108 nearest neighbor hopping, respectively. E_z arises from the buckling of 2D-Xenes and
 109 allows for tunability of their electronic properties.

110 When the SOC is not taken into account and no electric field is applied (Kane-Mele
 111 model¹⁰), silicene, germanene, and stanene are predicted to be zero-gap semiconductors
 112 with linear dispersions near the K and K' Dirac points. The computed Fermi velocities in
 113 silicene and germanene are about 6×10^5 m/s,^{6,11} roughly half of that for graphene. With
 114 SOC, silicene and germanene are predicted to be 2D TIs with bulk energy gaps of about
 115 1.5-2 meV and 23.9-30 meV, respectively.⁹ Stanene, owing to its stronger SOC,
 116 incorporates a 2D TI state with a sizeable energy gap of about 0.1 eV.^{12,13}

117 **The 2D-Xene experimental Odyssey.** The tendency of FS 2D-Xenes to buckle is
 118 experimentally confirmed by the *epitaxial growth* of various 2D-Xene “phases” on
 119 different substrates with *commensurate* surface lattice. An extensive list of substrates
 120 serving this purpose is enumerated in **Table 1**. Experimental identification of the buckled
 121 2D-Xene structure has been mainly based on scanning tunneling microscopy (STM)

122 assisted by *ab initio* atomic models. Other techniques such as angle resolved
123 photoemission spectroscopy (ARPES) have been used to reveal the electronic structure.
124 Starting from the ideal FS 2D-Xene lattice as predicted from *ab initio* simulations
125 (**Figure 1a**), a historical overview of the main experimental breakthroughs is presented in
126 **Figure 1** including the STM confirmation of silicene (**b**), closely paralleled by the
127 chemical synthesis of germanane (**c**), and followed by the epitaxy of germanene (**d**), the
128 realization of a silicene transistor (**e**) and the epitaxy of stanene (**f**).

129 The forerunner of the 2D-Xene roadmap is the epitaxial silicene on metallic
130 substrates.^{14,15-19} In particular, silicene-on-Ag(111) is interesting as a model of a buckled
131 elemental atomic sheet due to the wealth of commensurate phases on the host Ag(111)
132 surface.^{16,17} These phases are commonly written as $n\times n/m\times m$, where $n\times n$ and $m\times m$ refer
133 to the coincidence with the FS 2D-Xene lattice and the substrate lattice, respectively; they
134 arise from different rotational alignment of the 2D-Xene sheet with respect to the
135 substrate. STM topographies of the majority silicene phases are reported in **Figure 1b**
136 along with the respective atomic structure model. This structural versatility can
137 dramatically influence the electronic structure of each 2D-Xene phase, and is a general
138 monolayer property of the 2D-Xene family (**Table 1**).²⁰ In spite of this, substrate orbitals
139 strongly hybridize with the Si atoms, resulting in an overall metallic character of the
140 silicene-on-metal substrate system, as follows from ARPES investigations.^{11,21}

141 Following silicene, several STM studies have detailed the atomic arrangement of buckled
142 germanene phases on various metallic substrates^{22,23,24-26} (**Figure 1d**), and the epitaxy of
143 stanene on Bi₂Te₃ substrates has been established soon afterwards²⁷ (**Figure 1f**). Most
144 recently, the epitaxy of a 2D boron sheet, termed borophene, with a metallic character

145 ^{28,29} and of a monolayer of (silicene-like) phosphorene with semiconducting character³⁰
146 were respectively reported on Ag(111) and Au(111) substrates, thus extending the
147 realization of 2D-Xenes to elements beyond the group IVA atoms.

148 **Covalently functionalized 2D-Xenes.** The covalent functionalization into ligand-
149 terminated Xenes is an intriguing route towards tuning chemical, physical, and
150 topological properties of these materials, as well as increasing their environmental
151 stability. Here we define “Xanes” as 2D-Xene derivatives in which every atom on the
152 framework features a covalently bound ligand, thereby removing π -bonding. These
153 ligands directly couple to the half-filled p_z orbitals in 2D-Xenes, to produce a gapped,
154 semiconducting band structure, and the magnitude of this band gap depends on both the
155 framework element, and the identity of the covalent ligand.^{12,31,32} Unlike Xenes, Xanes
156 can be derived by topotactic exfoliation.³¹ The first reported example of topotactic
157 exfoliation of a single germanane sheet is shown in **Figure 1c**.

158 The most versatile route for preparing Xanes relies on the direct chemical conversion of
159 structurally related layered intermetallic “Zintl” phase precursors. For example, the
160 crystal structures of CaSi_2 , CaGe_2 , and BaSn_2 , are comprised of anionic $[\text{Si}]_n^-$, $[\text{Ge}]_n^-$,
161 and $[\text{Sn}]_n^-$ layers in a puckered honeycomb arrangement analogous to 2D-Xenes, with
162 each layer separated by a divalent cation. These phases can be transformed directly into
163 multi-layered van der Waals crystals of Xanes by reaction with an electrophilic species
164 that will bond directly to the group IVA framework and a solvent that solubilizes the
165 divalent cation. For instance, the reaction of CaSi_2 in aqueous HCl produces partially –
166 H/OH terminated silicane, a reaction first reported by Friedrich Wöhler in 1863.³³ In

167 aqueous acidic conditions, the Si- and Sn-based Xane frameworks become partially
168 terminated with -OH ligands, whereas the Ge-based frameworks are completely -H
169 terminated.^{31,32} Organic-terminated Xanes can be created via a similar one-step reaction
170 of precursor Zintl phases with alkyl halides. For instance, GeCH_3 has been prepared via
171 the direct reaction of CaGe_2 with CH_3I .³⁴ Also, some Si and Ge surface functionalization
172 routes can also graft ligands onto 2D Xanes, such as the hydrosilylation of alkenes and
173 alkynes onto 2D silicane.³⁵ Other strategies for preparing Xanes include electrochemical
174 atomic layer epitaxy, which has been shown to be a viable route towards germanane,³⁶ as
175 well as the H-chemisorption to 2D-Xenes.³⁷

176 The handful of emerging reports on the role of surface termination on electronic
177 properties of functionalized Xenes indicate that both the size and the electron-
178 donating/electron-withdrawing properties of the ligand have a strong influence on the
179 electronic structure. First, surface-terminating Xenes with ligands that have relatively
180 larger van der Waals radii can produce tensile strain in the 2D framework. This tensile
181 strain will lower the energy of the ligand-Si/Ge/Sn s-orbital antibonding levels at the
182 conduction band maximum (CBM), effectively reducing the band gap.¹² Increasing the
183 alkyl length by just a single methylene unit to ethyl ($\text{-CH}_2\text{CH}_3$) limits the fraction of
184 surface atoms that are functionalized with the organic substituent to functionalization to
185 80-85% whereas the remaining atoms are -H terminated.³⁸ While the framework of
186 functionalized Xenes might have the flexibility to accommodate the strain induced by
187 larger ligands, to date, GeCH_3 is the only synthesized Xene functionalization with nearly
188 uniform organic functionalization.³⁴ Second, more electronegative ligands will withdraw
189 electron density from the Xane framework, and similarly lower the energy of the ligand-

190 Si/Ge/Sn s-orbital antibonding levels at the CBM.³⁹ Consequently, replacing the –H
191 ligand in germanane with the more electron-donating –CH₃ ligand will increase the
192 observed band gap from 1.54 to 1.67.^{12,34} These Xenes can be in the form of multi-
193 layered crystals whose length and width is determined by the size of precursor Zintl
194 phases and can be greater than millimeters, suitable for exfoliation and further device
195 processing.³¹

196
197 **The triple S-factor in the epitaxial 2D-Xenes.** The experimental realization of the
198 epitaxial Xenes has been generally conditioned by three factors: Synthesis, Substrate, and
199 Stability. This *triple S-factor* brings several challenges for a full exploitation of Xene and
200 access to a broad range of characterization and/or applications. The synthesis of 2D-Xene
201 is restricted to expensive molecular beam epitaxy (MBE) methodologies requiring ultra-
202 high vacuum conditions. Moreover, substrates enabling the 2D-Xene epitaxy must be
203 commensurate with the FS 2D-Xene structure.^{14,15,16,17,19} Further efforts are in progress to
204 design or synthesize 2D-Xenes on weakly interacting substrates, and the option of
205 chalcogenide templates with a selected termination is promising to host a 2D-Xene
206 lattice.⁴⁰ This is the case of the growth of hexagonal silicene sheets on semiconducting
207 MoS₂.^{41,42} The option of Xenes on non-metallic substrates would bring obvious benefits
208 for device integration, scientific studies, and applications, and *substrate engineering* is a
209 demanding task of technological interest.

210 On the other hand, the chemical stability of 2D-Xenes under ambient condition is
211 severely restricted by the inherent thermodynamic preference of Si, Ge, and Sn for *sp*³
212 bonding. Air-stability issues can be overcome by making use of a non-destructive
213 encapsulation material such as Al₂O₃.⁴³

214 The case of silicene can be taken as a paradigmatic pathway to overcome the “triple S
215 factor” and develop a prototypical 2D-Xene nanoelectronic platform (**Figure 1e**). A
216 silicene sheet can be sandwiched in between two thin layers, the native Ag on one side
217 and Al₂O₃ encapsulation on the other side. The former layer comes from the delamination
218 of the "substrate", a cleavable Ag(111)-on-mica where the silicene is epitaxially grown.
219 The latter one is the stabilizing encapsulation sequentially deposited after silicene growth.
220 The “silicene sandwich” is easily handled as a sheet to be placed upside down on a
221 device-friendly platform, such as SiO₂/Si, and the top Ag patterned so as to obtain a Ag-
222 free silicene channel in between two (or more) "native" Ag electrodes, hence completing
223 a transistor device structure. Room temperature operation of this silicene transistor
224 revealed an ambipolar character in agreement with the predicted graphene-like nature of
225 the particular silicene phase in the experiment.⁴⁴ Despite the fast degradation of exposed
226 Ag-free silicene in ambient condition that is yet to be fully addressed, this transfer
227 methodology can be generally extended to the class of Xenes-on-substrate, and hence,
228 offer a universal route for verifying the quantum transport properties of Xenes.⁴⁵

229

230

231 **Topology as a paradigm shift for quantum electronics**

232 2D TIs support the intriguing quantum spin Hall (QSH) effect, characterized by
233 insulating bulk states with gapless helical edge states that are protected against back-
234 scattering by time reversal symmetry (**Figure 2a**). The QSH effect was first theoretically
235 predicted and subsequently experimentally observed in a HgTe quantum well.^{46,47}
236 Graphene was proposed to have the same effect,¹⁰ but its bulk gap is extremely small
237 (~μeV). The buckled 2D-Xenes have much larger QSH gaps (up to 0.3 eV),¹² suitable for

238 room-temperature usage, and their QSH states are tunable by chemical functionalization
239 from π orbital states to σ orbital states (**Figure 2b**).¹² This tunable topology affords an
240 electronic switch where the logic state is dictated by the topological phase transition
241 rather than by the charge depletion/inversion as in conventional semiconductors.

242 **The benefit of gaining weight.** 2D-Xenes share the same Dirac physics as
243 graphene, which is a 2D Dirac semimetal when excluding the SOC and becomes a QSH
244 insulator when including the SOC (**Figure 2b**, left).^{10,9,12} Notably, the SOC-induced bulk
245 gap in silicene (1.5-2 meV)^{45,9} is much larger than in graphene ($\sim\mu\text{eV}$). The underlying
246 mechanism is two-fold. The first-order contribution of SOC, which is turned off in a
247 planar structure like graphene, is turned on in silicene because the hybridization between
248 π and σ orbitals of nearest neighbors becomes allowed in a buckled structure.⁹ Moreover,
249 the SOC strength is commensurate with increasing weight. Thus enhanced SOC is
250 obtained in germanene (23.9-30.0 meV) and stanene ($\sim 0.1\text{eV}$).^{9,12,48} In perspective, the
251 QSH gap increases five orders of magnitude from graphene to stanene, compliments of
252 the heavier mass and structural buckling.

253 The chemical functionalization of 2D-Xenes provides an additional degree of freedom to
254 tune topological states. The saturation of the p_z orbitals opens a large energy gap at the K
255 and K' points, which destroys the Dirac physics of the π orbitals. The low-energy physics
256 is then determined by the σ orbitals around the Γ point (**Figure 2b**, right), where inverted
257 band structures may occur in 2D-Xenes composed of heavier elements.^{12,48} Take the
258 fluorinated stanene (F-stanene) as an example. The relevant states around the Fermi level
259 are comprised of s , p_x , and p_y orbitals on the Sn atoms, split into bonding and anti-
260 bonding states by the Sn-Sn interaction. Unlike undecorated graphene, the anti-bonding s

261 state is located below the bonding p_{xy} state at the Γ point, showing an inverted band order.
262 The s - p band inversion results in a nontrivial QSH phase,¹² similar to the scenario of the
263 HgTe quantum well.⁴⁶ Therefore, the QSH states are varied from π orbitals described by
264 the Kane-Mele model¹⁰ to σ orbitals described by the Bernevig-Hughes-Zhang model⁴⁶.
265 The new QSH states derived from σ orbitals possess many advantages^{12,48}. First, the QSH
266 gaps are extraordinarily large (up to 0.3 eV), since the effective SOC of σ orbitals is
267 significantly larger than that of π orbitals. Second, the electronic properties can be
268 controllably tuned. Functionalization with different chemical groups can result in
269 topologically distinct phases (**Figure 2c**). Moreover, applying external strain can
270 effectively control the emergence or disappearance of the helical edge states.
271 Third, in comparison with the π orbitals that are easily affected by substrate and
272 adsorbates,^{27,49} the σ orbitals that are composed of in-plane p_{xy} states are relatively more
273 environmentally stable. Even when forming chemical bonds with the substrate, large-gap
274 σ -orbital-derived QSH states are predicted to be preserved in functionalized stanane⁴⁰.
275 Given the dependence on external factors owing to their buckled nature, 2D-Xenes may
276 offer a high degree of functional versatility. For example, in silicene, physical influences
277 such as electric and magnetic fields, mechanical strain, and temperature has been
278 predicted to produce a variety of electronic states including semimetallic,
279 semiconducting, superconducting, and trivial insulating phases, in addition to about
280 *sixteen* 2D TI phases.⁵⁰ These TI phases arise from the combination of the four defining
281 topological numbers in a honeycomb lattice, which are the Chern, spin-Chern, valley-
282 Chern and spin-valley-Chern numbers with an end result of five types of topological
283 quantum states, namely the spin-polarized quantum anomalous Hall (SQAH), quantum

284 valley Hall (QVH) and quantum spin-valley Hall (QSVH) states in addition to the already
285 mentioned QSH and QAH states (**Figure 2d**).⁵¹

286

287 **A Buckled Outlook**

288 The interplay of non-trivial 2D topological features and the buckled structure of 2D-
289 Xenes may also open new routes for disruptive applications like low-energy electronics,
290 piezo-magnetism, enhanced thermoelectricity and spintronics.¹² Furthermore, by
291 explicitly breaking the symmetries (for example, gauge symmetry, inversion symmetry
292 and time reversal symmetry), new emerging physics (such as topological
293 superconductivity⁵², valley-polarized metal,⁴⁵ and QAH effect⁴⁵) can be explored in 2D-
294 Xenes.

295 **From digital to topological bits.** One of the more visionary outlook about 2D-Xenes is
296 the realization of a paradigm shift from conventional to quantum electronics based on
297 field-controllable topological properties. Transport through the QSH edge states can be
298 ballistic, thus promising an exceptional advance in terms of energy saving in electronic
299 devices. In contrast to carbon nanotubes or graphene where ballistic transport can be
300 affected by defects, transport in 2D-Xenes in the QSH regime is robust against scattering.
301 Equally appealing is the opportunity to access a logic functionality based on the concept
302 of topological phase transitions. A topological phase transition occurs when the QSH
303 state characterized by ballistic edge states that can serve as information carriers (“ON”
304 state) is switched to a trivial insulator state with vanishing conductance (“OFF” state) vis-
305 à-vis an external electric field E_z (**Figure 3a**, top diagram).⁵⁰ The two ON/OFF states
306 define a logic switch mechanism, namely a *topological bit*, which can be distinguished by

307 the sequential topological gap closing and trivial gap opening as a function of the external
308 field.

309 A prototypical device structure based on the gate bias modulation can be understood as a
310 *quantum* topological insulator field-effect transistor (TI-FET)⁵³ as shown in the
311 corresponding sketch of **Figure 3b**. The gate bias can be employed to switch the TI-FET
312 from the ON to the OFF state, whereas the drain-source voltage facilitates one kind of
313 helical carrier through each edge. Being topologically protected and helical in character,
314 the edge states in these quantum TI-FETs serve as truly one-dimensional, spin-polarized
315 dissipationless highways for charge transport that is robust against scattering from non-
316 magnetic material defects,¹² and potentially suitable for scaled low-power nanoelectronic
317 devices.

318 The main challenge with devices based on electric field-driven topological phase
319 transitions is the relatively large critical field required ($E_c = 2\lambda_{SO}/\delta$, where $2\lambda_{SO}$ is the
320 SOC induced bandgap), which is of the order of 0.05 V/nm and 1 V/nm for silicene and
321 stanene, respectively. In light of this, a *classical* TI-FET not predicated on topological
322 phase transitions was recently proposed.⁵⁴ In this scheme, the 2D TI is configured as a
323 nanoribbon FET with the width small enough to ensure inter-edge elastic scattering
324 (namely, within an order of magnitude of the field-dependent edge-bulk tunneling length
325 scale, ~ 1 nm for F-stanene and ten times larger in silicene). Unlike the conventional FET
326 where the field-effect enhances the carrier density and conductivity increases, the field-
327 effect in classical TI-FET facilitates phonon-mediated scattering of edge electrons into
328 bulk states by reducing the energy barrier and hence, conductivity decreases.

329 Alternatively, a topological phase transition can be driven by applying external strain in
330 functionalized 2D-Xenes because the *s-p* band inversion at the Γ point sensitively
331 depends on the interatomic bond length.¹² In this case, the details of the topological
332 phase transition depend on the identity of the functional group. For instance, F-stanene is
333 a QSH insulator that undergoes a transition to a trivial insulator state as a function of the
334 compressive strain (over a critical value of about -7%) thus nominally mimicking the
335 same ON/OFF sequence of the electric field induced topological phase transition (**Figure**
336 **3a**, middle diagram). Conversely, H-stanene is a trivial insulator at zero applied strain
337 and enters a QSH state when applying a tensile strain over a critical value of about 2%
338 thus manifesting an inverted OFF-ON logic mechanism (**Figure 3a**, bottom diagram).
339 Both mechanisms may open unprecedented routes for 2D-Xene-based piezotronic
340 devices (see the corresponding sketches in **Figure 3b**).

341 **New emerging applications.** The existence of large-gap, tunable and robust QSH
342 states make 2D-Xenes promising for various applications (**Figure 3c**). The large bulk gap
343 (~ 0.3 eV)¹² enables QSH phenomena to occur at room temperature. The helical edge
344 states are useful for low-energy electronics, since they can conduct electricity without
345 generating heat^{10,46,47}. They can also induce anomalous Seebeck effect due to the strong
346 energy dependence in lifetime introduced by the edge-bulk interaction.⁵⁵ The
347 thermoelectric performance of QSH insulators can be effectively improved by optimizing
348 the morphology to maximize the edge-state contribution.⁵⁵ In addition, the helical edge
349 states may also find important applications in spintronics (for example in spin transfer
350 torque, spin Seebeck, spin-charge conversion, and spin-filter⁵⁶ based devices). However,
351 very little experimental progress has been achieved until now, mainly because high-

352 quality samples are still lacking.²⁷ More experimental effort is thus essential to advance
353 2D-Xenes and related materials, and ultimately realize the above-mentioned concepts.

354 **New emerging physics.** 2D-Xenes may also offer an ideal platform to study new
355 emerging physics. Exotic quantum effects would emerge upon explicitly breaking
356 different symmetries in 2D-Xenes (**Figure 3c**). For instance, breaking the *inversion*
357 *symmetry* by substrate or electric field introduces the Rashba effect, which enables the
358 spin manipulation as well as access to topological superconductivity.⁵² Breaking *time*
359 *reversal symmetry* by magnetism^{40,57} may induce the QAH effect, which supports chiral
360 edge states that are topologically protected against scattering. A near room-temperature
361 QAH effect has been predicted in half-functionalized stanene and germanene, where a
362 ferromagnetic order is formed between local magnetic moments of unsaturated p_z states.⁵⁷
363 Breaking *gauge symmetry* by superconductivity may afford exotic topological
364 superconducting states bearing Majorana fermions that are useful for fault-tolerant
365 topological quantum computation.⁵²

366 Even richer physics is expected by breaking different symmetries simultaneously. For
367 instance, the use of an electric field together with an exchange field ΔM (from magnetic
368 impurities or by proximity coupling with a ferromagnet) enables tuning the spin and
369 valley degrees of freedom independently, which generates a variety of phases in 2D-
370 Xenes.⁴⁵ Furthermore, the symmetries can be broken either globally or locally. The local
371 symmetry breaking, though preserving the topology, can considerably affect properties of
372 the QSH states. As an example, the helical edge states are eliminated when introducing
373 an in-plane ferromagnetic order to the edge atoms. The existence of the helical edge

374 states thus can be controlled by local edge manipulation, which leads to potential
375 applications in giant magnetoresistance and an ideal spin filter.⁵⁶

376 **Perspective**

377 By virtue of their buckled character, 2D-Xenes can potentially serve as a nanotechnology
378 platform with multiple physical features for fundamental research and applications. The
379 diverse material properties in intrinsic and functionalized Xenes permit a wide degree of
380 freedom in designing efficient, on-demand or reconfigurable devices for electronic,
381 spintronic, photonic, thermal, energy, mechanical, chemical and sensor nanosystems.
382 However, many processing and technological issues are yet to be solved, the most
383 significant of which is the instability in ambient conditions which complicates the
384 establishment of scalable routes for device integration schemes. Appropriate solutions
385 including the design of device-friendly and neutral substrates, and the development of
386 large-scale production methodologies (for example chemical vapor deposition) are
387 demanding issues for a viable Xene nanotechnology. Nonetheless, the recently reported
388 technological and synthetic advances are encouraging towards the exploration of the
389 unique topological phenomena in 2D-Xenes and their exploitation in innovative device
390 concepts.

391

392

393 **Acknowledgements**

394 The Authors are grateful for fruitful discussions with Dr. C. Grazianetti, E. Cinquanta,
395 Dr. L. Tao, Prof. M. Fanciulli, Prof. V.V. Afanas'ev, Prof. A. Stesmans, Prof. William
396 Vandenberghe, Prof. M. Fischetti, Dr. A. Dimoulas, Dr. D. Tsoutsou, and Prof. Motohiko
397 Ezawa. The Authors thank Jo Wozniak of UT-Austin TACC center for the renderings of
398 Fig. 3. A.M. is partially supported by the CNR under the grant "Laboratori Congiunti"
399 (SFET project). J.G. acknowledges partial support from the Center for Emergent
400 Materials: an NSF MRSEC under award number DMR-1420451, partial support from
401 NSF EFRI-1433467, and the Camille and Henry Dreyfus Foundation. M.H acknowledges
402 financial support from the KU Leuven Research Funds, project GOA/13/011. A.M. and
403 M.H. also acknowledge partial financial support from the EU-FP7 FET-Open grant no.
404 270749 ("2D-Nanolattices" project). Y.X. acknowledges support from Tsinghua
405 University Initiative Scientific Research Program and the National Thousand-Young-
406 Talents Program. S.C.Z. is supported by the Department of Energy, Office of Basic
407 Energy Sciences, Division of Materials Sciences and Engineering, under contract DE-
408 AC02-76SF00515 and by FAME, one of six centers of STARnet, a Semiconductor
409 Research Corporation program sponsored by MARCO and DARPA. D.A acknowledges
410 support from the Army Research Office (ARO), the Presidential Early Career Award for
411 Engineers and Scientists (PECASE), and the Gordon and Betty Moore Foundation.

412

413

414

415

416 **Item Captions**

417 **Table 1. Properties of 2D-Xenes.** Computed structural parameters of FS 2D-Xenes,
418 using first-principles calculations based on density functional theory (left-hand side).
419 Experimentally observed or calculated structural parameters of epitaxial Xenes-on-
420 substrates (right-hand side). a_x , ℓ_{x-x} , and δ are the cell lattice constant, interatomic
421 distance, and buckling parameter in 2D-Xenes. E_g is the SOC-induced band gap. The
422 latter branch includes a list of substrates that have been found to accommodate specific
423 2D-Xene lattices and their atomic reconstructions (commonly denoted as “phases”) on
424 the substrates’ surface. Graphene parameters are reported for comparison. Note that
425 graphene has nominally zero atomic buckling in the absence of rippling.

426

427 **Figure 1: The 2D-Xene Odyssey.** An evolutionary overview of the key-
428 experimental evidences of 2D-Xenes. (a) Atomic configuration of a FS 2D-Xene lattice
429 (top: side view, bottom: perspective view) where red and orange spheres represent X
430 atoms at top and bottom positions, respectively. (b) Silicene epitaxy on Ag(111)
431 substrates as a representative case of Xene-on-substrate systems. STM investigations of
432 Silicene-on-Ag(111) has revealed a multiphase character. Left: The STM topographies of
433 three majority phases, $3\times 3/4\times 4$, $\sqrt{7}\times\sqrt{7}/\sqrt{13}\times\sqrt{13}$, and $\sqrt{7}\times\sqrt{7}/2\sqrt{3}\times 2\sqrt{3}$, are reported
434 along with the atomic structure models. (c) Topotactic exfoliation of germanane as a first
435 example of the chemical exfoliation of a Xene sheet: process schematics (left) and optical
436 microscopy image of a single hydrogen-terminated germanane sheet (right). (d)
437 Representative case of germanene on metal substrates: STM topography of an extended

438 germanene sheet on Al(111) assisted by an *ab initio* atomic model. Adapted from Ref.²⁴.
439 (e) Silicene integration into a transistor device after Ref.⁴⁴: Silicene is epitaxially grown
440 on a cleavable Ag-on-mica substrate via MBE, encapsulated with a protective Al₂O₃ and
441 then delaminated as a Al₂O₃/silicene/Ag sandwich sheet; this “silicene sandwich” is
442 transferred to a device-friendly substrate (such as SiO₂/Si) and then integrated as the
443 active channel in a field-effect transistor structure by patterning the native Ag to make
444 contact electrodes. (f) Epitaxy of stanene on Bi₂Te₃ substrates based on STM
445 identification of a buckled and unreconstructed lattice structure. Adapted from Ref.²⁷.

446

447 **Figure 2: Topology as a paradigm shift in nanoelectronics.** **a)** Top view of a 2D-
448 Xene in a QSH state bearing helical currents at the edges. **b)** Side view of the atomic
449 structure and molecular orbital, and the low-energy bands with (red solid lines) and
450 without (black dashed lines) spin-orbit coupling for pure (left) and functionalized (right)
451 Xene. The red and blue spheres denote atoms of different sublattices, and the white
452 spheres denote the chemical functional group. **c)** Energy gap as a function of the lattice
453 constant induced by the covalent functionalization of stanene. Adapted from Ref.¹². **d)**
454 The topological phase diagram as a function of perpendicular electric field E_z and the
455 exchange field ΔM , and the arrows reflect the spin polarization. Adapted from Ref.⁵¹

456

457 **Figure 3: The topological bit and emerging physics based on broken symmetry.**
458 **a)** Schematic band structure diagrams of nanoribbons along the 1D Brillouin zone (Γ -X',
459 X' is a k -point point along the nanoribbon length direction) for (top) bare stanene,
460 (middle) and fluorine-terminated (SnF), and (bottom) hydrogen-terminated (SnH) stanane

461 and topological phase transitions induced by an out-of-plane electric field or a
462 compressive/tensile strain. The helical edge states that emerge within the bulk gap are
463 denoted by red lines. **b)** Corresponding sketches of a *quantum* TI-FET driven by an
464 electric field, by a compressive strain, and by a tensile strain. A 2D-Xene ribbon is
465 embedded in between a top gate and a substrate (for applying V_G), and source (S) and
466 drain (D) electrodes. **c)** Applications of the QSH states and new emerging physics
467 induced by breaking symmetries, including the A-B sublattice symmetry, inversion
468 symmetry P , time reversal symmetry T and gauge symmetry U .

469

470

471

472

473

474

475

476

477

478

479

480

481

482

483

	FS 2D-Xenes (predicted)					Epitaxial 2D-Xenes (Xene-on-substrate)					
	a_x (Å)	ℓ_{x-x} (Å)	δ (Å)	E_g	Ref.	substrate	phase	a_x (Å)	ℓ_{x-x} (Å)	δ (Å)	Ref.
Graphene	2.47	1.42	0	~1 μ eV		metals		2.47	1.42	0	58
Silicene	3.87	2.28	0.44	1.5-2 meV	59	Ag(111)	3 \times 3/4 \times 4	11.78	2.34-2.39	0.71-0.79	14,15 , 16,17
							$\sqrt{7}\times\sqrt{7}/\sqrt{13}\times\sqrt{13}$	10.60	2.31-2.36	0.77-0.79	
							$\sqrt{7}\times\sqrt{7}/2\sqrt{3}\times2\sqrt{3}$	10.20	2.28-2.37	1.10	
						Ir(111)	$\sqrt{3}\times\sqrt{3}/\sqrt{7}\times\sqrt{7}$	7.20	2.10	0.83	18
						ZrB ₂	$\sqrt{3}\times\sqrt{3}/2\times2$	6.72-6.78	2.24-2.26	0.90-1.35	19
					MoS ₂	1 \times 1/1 \times 1	3.17	2.61	1.90	41	
Germanene	4.06	2.44	0.69	23.9-30.0 meV	59	Au(111)	$\sqrt{3}\times\sqrt{3}/\sqrt{7}\times\sqrt{7}$	7.65	2.55	0.47	22
						Pt(111)	3 \times 3/ $\sqrt{19}\times\sqrt{19}$	12.0	~2.31	0.60	23
						Al(111)	2 \times 2/3 \times 3	8.50	2.58	1.23	24
						MoS ₂	1 \times 1/1 \times 1	3.82	2.20	0.86	42
						hex-AlN	3 \times 3/4 \times 4	12.31	2.37	0.70	26
Stanene	4.68	2.83	0.85	0.1 eV	12	Bi ₂ Te ₃	1 \times 1/1 \times 1	4.38	2.80	1.20	27

485

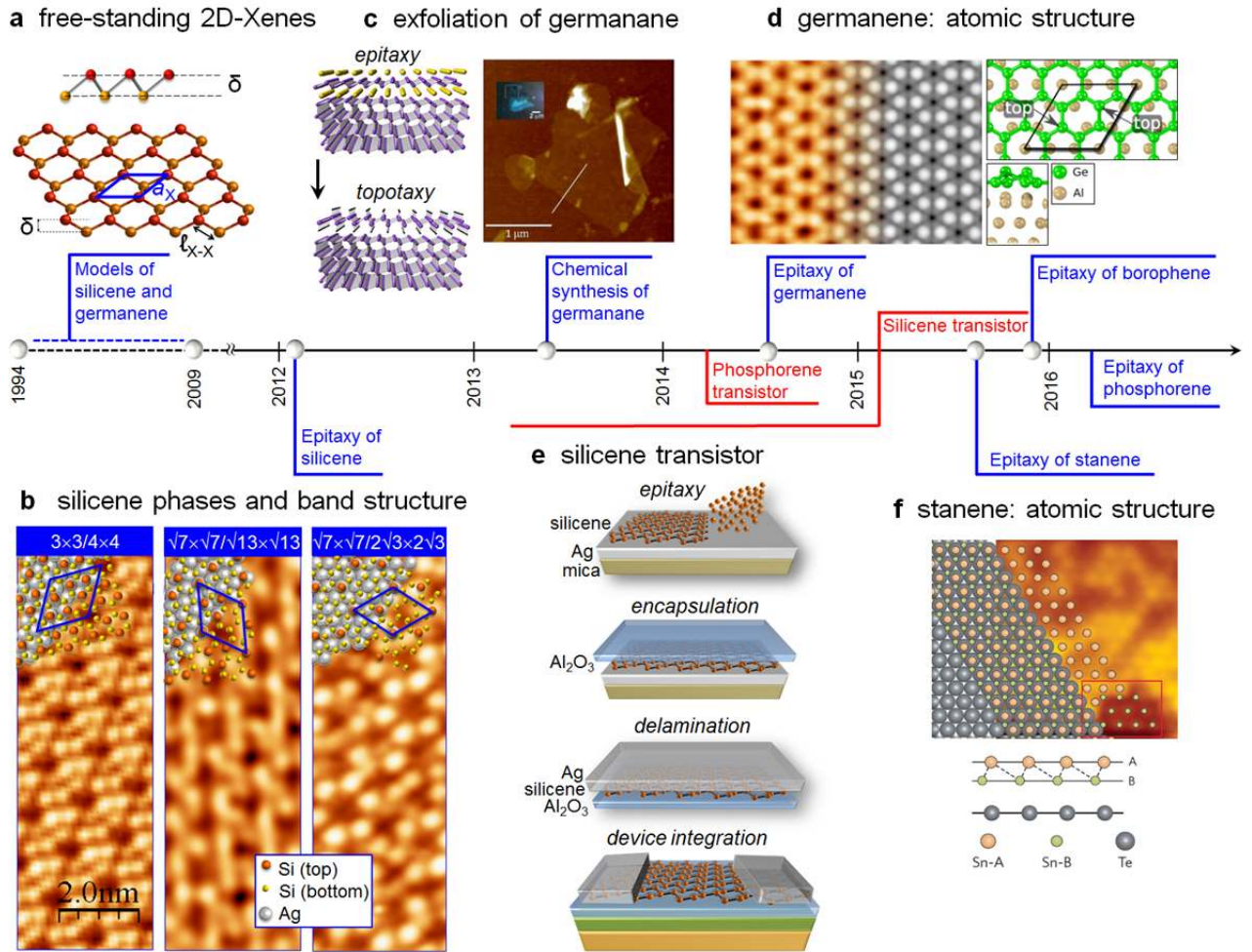
486

487

488 **Table 1**

489

490



491

492

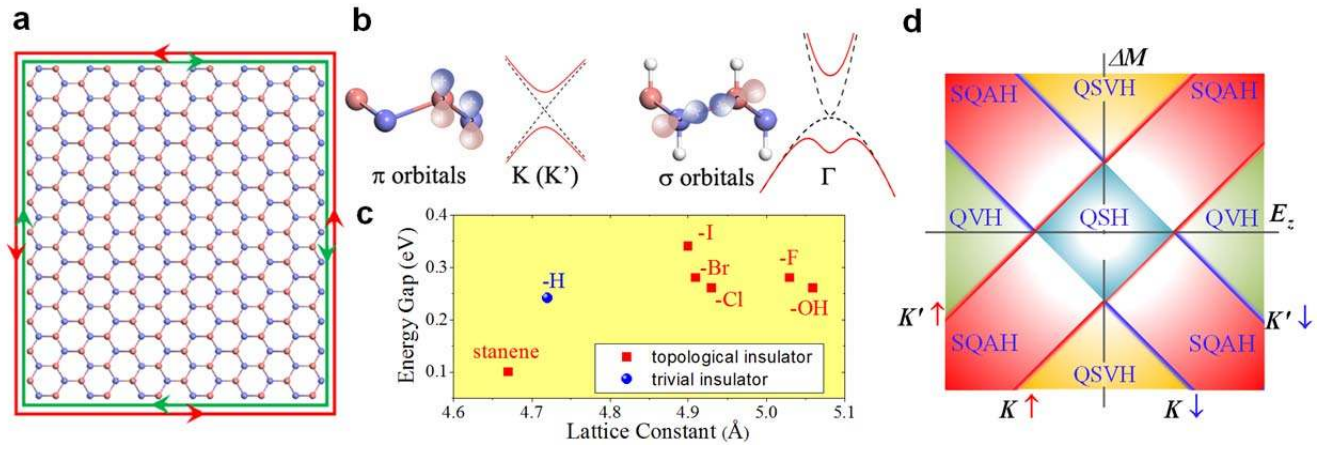
493

494

495 **Figure 1**

496

497



498

499

500

501

502

503 **Figure 2**

504

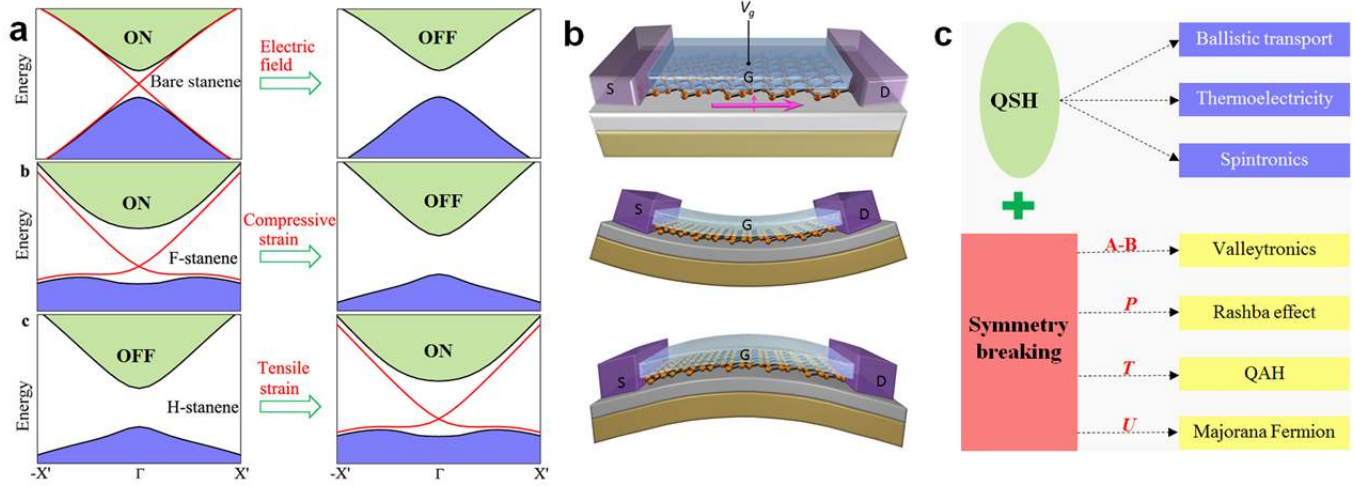
505

506

507

508

509



510

511 **Figure 3**

512

513

514

515

516

517

518

519

520

521

522

523

524 **List of References**

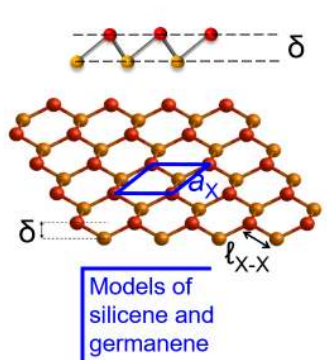
- 525 ¹ G Fiori, F Bonaccorso, G Iannaccone, T Palacios, D Neumaier, A Seabaugh, SK
526 Banerjee, and L Colombo, *Nature Nanotechnology* **9** (10), 768 (2014).
- 527 ² AC Ferrari, F Bonaccorso, V Fal'ko, KS Novoselov, S Roche, P Boggild, S
528 Borini, FHL Koppens, V Palermo, N Pugno, JA Garrido, R Sordan, A Bianco, L
529 Ballerini, M Prato, E Lidorikis, J Kivioja, C Marinelli, T Ryhanen, A Morpurgo,
530 JN Coleman, V Nicolosi, L Colombo, A Fert, M Garcia-Hernandez, A Bachtold,
531 GF Schneider, F Guinea, C Dekker, M Barbone, ZP Sun, C Galiotis, AN
532 Grigorenko, G Konstantatos, A Kis, M Katsnelson, L Vandersypen, A Loiseau, V
533 Morandi, D Neumaier, E Treossi, V Pellegrini, M Polini, A Tredicucci, GM
534 Williams, BH Hong, JH Ahn, JM Kim, H Zirath, BJ van Wees, H van der Zant, L
535 Occhipinti, A Di Matteo, IA Kinloch, T Seyller, E Quesnel, XL Feng, K Teo, N
536 Rupesinghe, P Hakonen, SRT Neil, Q Tannock, T Lofwandra, and J Kinaret,
537 *Nanoscale* **7** (11), 4598 (2015).
- 538 ³ Akinwande D, Tao L, Yu Q, Lou X, Peng P, and Kuzum D, *IEEE*
539 *Nanotechnology Magazine* **9**, 6 (2015).
- 540 ⁴ S Balendhran, S Walia, H Nili, S Sriram, and M Bhaskaran, *Small* **11**, 640
541 (2015).
- 542 ⁵ K Takaeda and K Shiraishi, *Physical Review B* **50**, 14916 (1994).
- 543 ⁶ S Cahangirov, M Topsakal, E Akturk, H Sahin, and S Ciraci, *Physical Review*
544 *Letters* **102**, 236804 (2009).
- 545 ⁷ GG Guzman-Verri and LCLY Voon, *Physical Review B* **76**, 075131 (2007).
- 546 ⁸ Carlo Grazianetti, Eugenio Cinquanta, and Alessandro Molle, *2d Materials* **3** (1)
547 (2016).
- 548 ⁹ CC Liu, WX Feng, and YG Yao, *Physical Review Letters* **107** (7), 076802
549 (2011).
- 550 ¹⁰ CL Kane and EJ Mele, *Physical Review Letters* **95**, 146802 (2005).
- 551 ¹¹ M Houssa, A Dimoulas, and A Molle, *Journal of Physics-Condensed Matter* **27**,
552 253002 (2015).
- 553 ¹² Y Xu, BH Yan, HJ Zhang, J Wang, G Xu, PZ Tang, WH Duan, and SC Zhang,
554 *Physical Review Letters* **111**, 136804 (2013).
- 555 ¹³ B van den Broek, M Houssa, E Scalise, G Pourtois, VV Afanas'ev, and A
556 Stesmans, *2D Materials* **1**, 021004 (2014).
- 557 ¹⁴ P Vogt, P De Padova, C Quaresima, J Avila, E Frantzeskakis, MC Asensio, A
558 Resta, B Ealet, and G Le Lay, *Physical Review Letters* **108**, 155501 (2012).
- 559 ¹⁵ CL Lin, R Arafune, K Kawahara, N Tsukahara, E Minamitani, Y Kim, N Takagi,
560 and M Kawai, *Applied Physics Express* **5**, 045802 (2012).
- 561 ¹⁶ BJ Feng, ZJ Ding, S Meng, YG Yao, XY He, P Cheng, L Chen, and KH Wu,
562 *Nano Letters* **12**, 3507 (2012).
- 563 ¹⁷ Daniele Chiappe, Carlo Grazianetti, Grazia Tallarida, Marco Fanciulli, and
564 Alessandro Molle, *Advanced Materials* **24**, 5088 (2012).
- 565 ¹⁸ L Meng, YL Wang, LZ Zhang, SX Du, RT Wu, LF Li, Y Zhang, G Li, HT Zhou,
566 WA Hofer, and HJ Gao, *Nano Letters* **13**, 685 (2013).
- 567 ¹⁹ A Fleurence, R Friedlein, T Ozaki, H Kawai, Y Wang, and Y Yamada-Takamura,
568 *Physical Review Letters* **108**, 245501 (2012).

569 20 E Scalise, E Cinquanta, M Houssa, B van den Broek, D Chiappe, C Grazianetti, G
570 Pourtois, B Ealet, A Molle, M Fanciulli, VV Afanas'ev, and A Stesmans, *Applied*
571 *Surface Science* **291**, 113 (2014).
572 21 Tsoutsou D, Xenogiannopoulou E, Golias E, Tsipas P, and Dimoulas A, *Applied*
573 *Physics Letters* **103**, 231604 (2013).
574 22 ME Davila, L Xian, S Cahangirov, A Rubio, and G Le Lay, *New Journal of*
575 *Physics* **16**, 095002 (2014).
576 23 LF Li, SZ Lu, JB Pan, ZH Qin, YQ Wang, YL Wang, GY Cao, SX Du, and HJ
577 Gao, *Advanced Materials* **26**, 4820 (2014).
578 24 M Derivaz, D Dentel, R Stephan, MC Hanf, A Mehdaoui, P Sonnet, and C Pirri,
579 *Nano Letters* **15**, 2510 (2015).
580 25 P Bampoulis, L Zhang, A Safaei, R van Gastel, B Poelsema, and HJW Zandvliet,
581 *Journal of Physics-Condensed Matter* **26**, 442001 (2014).
582 26 F D'Acapito, S Torrenzo, E Xenogiannopoulou, P Tsipas, J Marquez Velasco, D
583 Tsoutsou, and A Dimoulas, *Journal of Physics - Condensed Matter* (2016).
584 27 FF Zhu, WJ Chen, Y Xu, CL Gao, DD Guan, CH Liu, D Qian, SC Zhang, and JF
585 Jia, *Nature Materials* **14**, 1020 (2015).
586 28 AJ Mannix, XF Zhou, B Kiraly, JD Wood, D Alducin, BD Myers, XL Liu, BL
587 Fisher, U Santiago, JR Guest, MJ Yacaman, A Ponce, AR Oganov, MC Hersam,
588 and NP Guisinger, *Science* **350** (6267), 1513 (2015).
589 29 Baojie Feng, Jin Zhang, Qing Zhong, Wenbin Li, Shuai Li, Hui Li, Peng Cheng,
590 Sheng Meng, Lan Chen, and Kehui Wu, *Nat Chem advance online publication*
591 (2016).
592 30 Jia Lin Zhang, Songtao Zhao, Cheng Han, Zhunzhun Wang, Shu Zhong, Shuo
593 Sun, Rui Guo, Xiong Zhou, Cheng Ding Gu, Kai Di Yuan, Zhenyu Li, and Wei
594 Chen, *Nano Letters* (2016).
595 31 Elisabeth Bianco, Sheneve Butler, Shishi Jiang, Oscar D. Restrepo, Wolfgang
596 Windl, and Joshua E. Goldberger, *Acs Nano* **7**, 4414 (2013).
597 32 Shishi Jiang, Maxx Q. Arguilla, Nicholas D. Cultrara, and Joshua E. Goldberger,
598 *Accounts of Chemical Research* **48** (1), 144 (2015).
599 33 F. Wohler, *Justus Liebigs Annalen der Chemie* **127** (3), 257 (1863).
600 34 Shishi Jiang, Sheneve Butler, Elisabeth Bianco, Oscar D. Restrepo, Wolfgang
601 Windl, and Joshua E. Goldberger, *Nature Communications* **5**, 3389 (2014).
602 35 Hideyuki Nakano, Mitsuru Nakano, Koji Nakanishi, Daiki Tanaka, Yusuke
603 Sugiyama, Takashi Ikuno, Hirotaka Okamoto, and Toshiaki Ohta, *Journal of the*
604 *American Chemical Society* **134** (12), 5452 (2012).
605 36 XH Liang, QH Zhang, MD Lay, and JL Stickney, *Journal of the American*
606 *Chemical Society* **133** (21), 8199 (2011).
607 37 Qiu J, Fu X, Xu Y, Zhou Q, Meng S, Li H, Chen L, and Wu K, (*ACS Nano*,
608 2015), Vol. 9, pp. 11192.
609 38 Hongbin Yu, Lauren J. Webb, Santiago D. Solares, Peigen Cao, William A.
610 Goddard, III, James R. Heath, and Nathan S. Lewis, *Journal of Physical*
611 *Chemistry B* **110**, 23898 (2006).
612 39 CG van de Walle and JE Northrup, *Physical Review Letters* **70**, 1116 (1993).
613 40 Y Xu, PZ Tang, and SC Zhang, *Physical Review B* **92**, 081112 (2015).

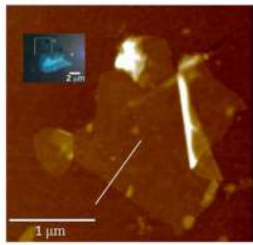
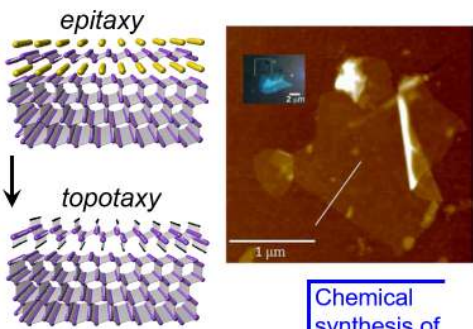
614 41 D Chiappe, E Scalise, E Cinquanta, C Grazianetti, B van den Broek, M Fanciulli,
615 M Houssa, and A Molle, *Advanced Materials* **26** (13), 2096 (2014).
616 42 L. Zhang, P. Bampoulis, A. N Rudenko, Q. Yao, A. van Houselt, B. Poelsema,
617 M. I Katsnelson, and H. J W Zandvliet, *Physical Review Letters* **116** (25),
618 256804 (2016).
619 43 A Molle, C Grazianetti, D Chiappe, E Cinquanta, E Cianci, G Tallarida, and M
620 Fanciulli, *Advanced Functional Materials* **23** (35), 4340 (2013).
621 44 L Tao, E Cinquanta, D Chiappe, C Grazianetti, M Fanciulli, M Dubey, A Molle,
622 and D Akinwande, *Nature Nanotechnology* **10** (3), 227 (2015).
623 45 M Ezawa, *Physical Review Letters* **109**, 055502 (2012).
624 46 BA Bernevig, TL Hughes, and SC Zhang, *Science* **314**, 1757 (2006).
625 47 M Konig, S Wiedmann, C Brune, A Roth, H Buhmann, LW Molenkamp, XL Qi,
626 and SC Zhang, *Science* **318**, 766 (2007).
627 48 C Si, JW Liu, Y Xu, J Wu, BL Gu, and WH Duan, *Physical Review B* **89**,
628 115429 (2014).
629 49 PZ Tang, PC Chen, WD Cao, HQ Huang, S Cahangirov, LD Xian, Y Xu, SC
630 Zhang, WH Duan, and A Rubio, *Physical Review B* **90** (12) (2014).
631 50 Motohiko Ezawa, *Journal of the Physical Society of Japan* **84** (12), 121003
632 (2015).
633 51 M Ezawa, *Physical Review B* **87**, 155415 (2013).
634 52 J Wang, Y Xu, and SC Zhang, *Physical Review B* **90**, 054503 (2014).
635 53 M Ezawa, *Applied Physics Letters* **102**, 172103 (2013).
636 54 WG Vandenberghe and MV Fischetti, *Journal of Applied Physics* **116**, 173707
637 (2014).
638 55 Y Xu, ZX Gan, and SC Zhang, *Physical Review Letters* **112**, 226801 (2014).
639 56 S Rachel and M Ezawa, *Physical Review B* **89**, 195303 (2014).
640 57 SC Wu, GC Shan, and BH Yan, *Physical Review Letters* **113**, 256401 (2014).
641 58 J Wintterlin and ML Bocquet, *Surface Science* **603** (10-12), 1841 (2009).
642 59 E Scalise, M Houssa, G Pourtois, B van den Broek, V Afanas'ev, and A Stesmans,
643 *Nano Research* **6** (1), 19 (2013).
644
645
646
647
648
649
650

	Free-standing Xenes (predicted)					Epitaxial Xenes (Xene-on-substrate)						
	a_X (Å)	ℓ_{X-X} (Å)	δ (Å)	E_g	Ref.	substrate	phase	a_X (Å)	ℓ_{X-X} (Å)	δ (Å)	Ref.	
Graphene	2.47	1.42	0	~ 1 μeV		metals		2.47	1.42	0	58	
Silicene	3.87	2.28	0.44	1.5-2 meV	59	Ag(111)	$3\times 3/4\times 4$	11.78	2.34- 2.39	0.71- 0.79	14,15, 16,17	
							$\sqrt{7}\times\sqrt{7}/\sqrt{13}\times\sqrt{13}$	10.60	2.31- 2.36	0.77- 0.79		
							$\sqrt{7}\times\sqrt{7}/2\sqrt{3}\times 2\sqrt{3}$	10.20	2.28- 2.37	1.10		
							Ir(111)	$\sqrt{3}\times\sqrt{3}/\sqrt{7}\times\sqrt{7}$	7.20	2.10	0.83	18
							ZrB ₂	$\sqrt{3}\times\sqrt{3}/2\times 2$	6.72- 6.78	2.24- 2.26	0.90- 1.35	19
							MoS ₂	$1\times 1/1\times 1$	3.17	2.61	1.90	41
Germanene	4.06	2.44	0.69	23.9- 30.0 meV	59	Au(111)	$\sqrt{3}\times\sqrt{3}/\sqrt{7}\times\sqrt{7}$	7.65	2.55	0.47	22	
						Pt(111)	$3\times 3/\sqrt{19}\times\sqrt{19}$	12.0	~ 2.31	0.60	23	
						Al(111)	$2\times 2/3\times 3$	8.50	2.58	1.23	24	
						MoS ₂	$1\times 1/1\times 1$	3.82	2.20	0.86	42	
						hex-AlN	$3\times 3/4\times 4$	12.31	2.37	0.70	26	
Stanene	4.68	2.83	0.85	0.1 eV	12	Bi ₂ Te ₃	$1\times 1/1\times 1$	4.38	2.80	1.20	27	

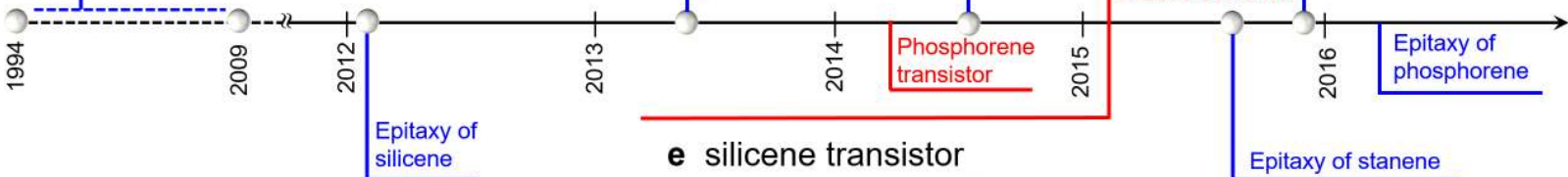
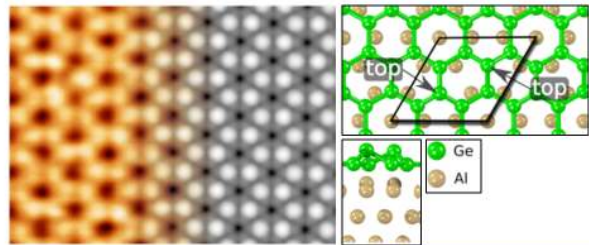
a free-standing 2D-Xenes



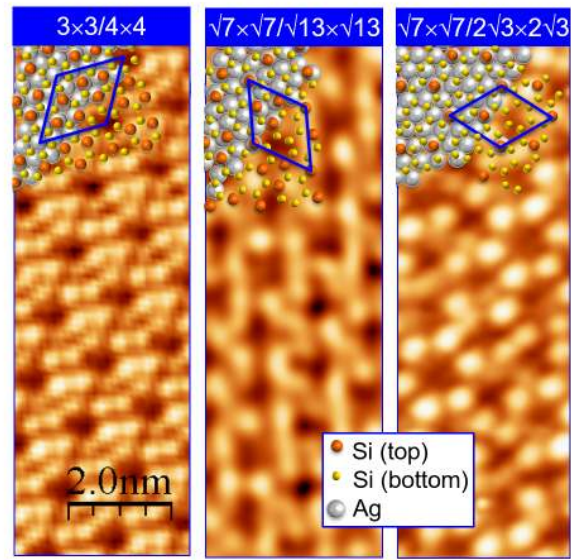
c exfoliation of germanane



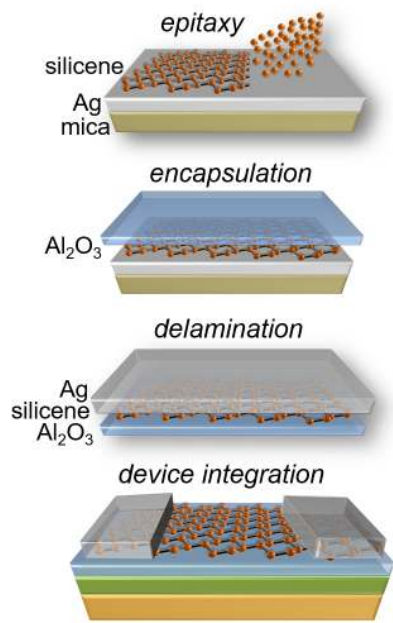
d germanene: atomic structure



b silicene phases and band structure



e silicene transistor



f stanene: atomic structure

